EARTH SCIENCES
RESEARCH JOURNAL
Earth Sci. Res. J. Vol. 27, No. 4 (December, 2023): 327 - 341

UNIVERSIDAD NACIONAL DE COLOMBIA

GEOLOGY

A contribution to the understanding of the origin of the Ginebra Gold District mineralizations, Colombia

Bibiana P. Rodríguez-Ramos, Juan C. Molano and Camilo, E. Dorado
Universidad Nacional de Colombia
Departamento de Geociencias
*Corresponding author: bprodriguezr@unal.edu.co

ABSTRACT

Ginebra´s gold mineralization is hosted by the Ginebra Ophiolitic Massif and the Buga Batholith, in the western flank of the Central Cordillera of Colombia. Gold occurs as disseminations, quartz-carbonate stockwork veinlets and quartz lodes with a strong structural control and are composed by small amounts of sulfides, mostly pyrite, with galena, sphalerite and chalcopyrite in at least two different deposition events and related to strong sericite-chlorite-epidote haloes, indicative of near-neutral and reduced fluids. Petrography and Raman spectroscopy allowed to identify two main fluid inclusions assemblages primary to pseudo-secondary in origin, both of them aqueous and CO_2-rich, with variable N_2. Microthermometric analysis indicates the hydrothermal fluids associated with the gold were low saline (0.75-6.22 wt% NaCl equiv.) and presented a minimum trapping temperature ranging from 237.4 to 301.6°C. Petrography and microthermometric results suggest an isothermal fluid mixing and/or H_2S loss as the main mechanisms related to gold bi-sulfide/thio-sulfide complexes destabilization and precipitation. Sulfur isotopes indicates a close to zero range (-8.2-+4.8‰), suggesting a restricted fluid circulation through the magmatic rocks of the Buga Batholith and the Ginebra Ophiolitic Massif. Besides, the oxygen and deuterium isotopes from hydrothermal sericite and chlorite accompanying to gold events, indicates a metamorphic origin for the hydrothermal fluids. ^{40}Ar-^{39}Ar dating of the hydrothermal alteration haloes, from El Retiro and La Esperanza, indicates a late Cretaceous-Paleocene age, between 67 and 65 Ma, contemporaneous with a regional strong dextral transpressive deformation related to subduction to obduction and exotic terrane accretion against the north-western part of the South American Plate. Although the hydrothermal fluid characteristics of the Ginebra Gold Disctrict are compatible with both the Intrusion-Related and Orogenic Gold deposit types, the metamorphic nature of the hydrothermal fluids and the tectonic regime at the time of mineralization event, allow us to propose they are compatible with an Orogenic Gold deposit.

Keywords: Fluid Inclusions; Microthermometry; Raman Spectroscopy; Late Cretaceous; Orogenic Gold.

Contribución al estudio del origen de las mineralizaciones auríferas de Ginebra, en Colombia

RESUMEN

Las mineralizaciones del Distrito Aurífero de Ginebra están emplazadas tanto en el Macizo Ofiolítico de Ginebra como en el Batolito de Buga, en el flanco occidental de la cordillera Central de Colombia. Corresponden a diseminaciones, stockwork de vetillas y vetas de cuarzo-carbonato, estas últimas con fuerte control estructural, bajas cantidades de sulfuros (>pirita-galena-esfalerita-calcopirita), al menos dos eventos de depósito de oro y desarrollo de halos de alteración fuerte (sericita-clorita-epidota). Análisis petrográficos y de espectroscopía Raman identificaron dos ensamblajes de inclusiones fluidas principales, primario y pseudo-secundario, ambos acuosos y ricos en CO_2, con cantidades variables de N_2. Los análisis microtermométricos indican fluidos hidrotermales con salinidad baja a moderada (0.75-6.22wt% NaCl equiv.) y temperatura mínima de entrampamiento entre 237.4 y 301.6°C. Asimismo, sugieren que un proceso de mezcla isotermal de fluidos y/o de pérdida de H_2S fueron los mecanismos responsables de la desestabilización de los complejos bi-sulfurados/thio-sulfurados en los que se transportó el oro y produjeron su depósito. Isótopos de azufre (entre -8.2 y +4.8‰) sugieren una circulación restringida de los fluidos hidrotermales por las rocas del macizo y del batolito. Adicionalmente, isótopos de oxígeno y deuterio en sericita y clorita hidrotermal, que acompañan la mineralización, reflejan un origen metamórfico para estos fluidos. Dataciones ^{40}Ar-^{39}Ar en los halos de alteración de las estructuras de El Retiro y La Esperanza, indican una edad entre 65 y 67 Ma, contemporánea con una deformación regional transpresiva dextral, relacionada con subducción a obducción y acreción de terrenos exóticos contra la margen nor-occidental de la placa Sudamericana. Aunque las características de los fluidos hidrotermales de las mineralizaciones son compatibles tanto con depósitos de tipo "Intrusion-Related" y Oro Orogénico, su naturaleza metamórfica y el régimen tectónico existente al momento del evento mineralizante, permite proponer que son compatibles con un depósito de tipo Oro Orogénico más que un "Intrusion-Related".

Palabras clave: Inclusiones Fluidas; Microtermometría; Espectroscopía Raman; Cretácico Tardío; Oro Orogénico.

Record
Manuscript received: 31/05/2022
Accepted for publication: 30/01/2024

How to cite item:
Rodriguez-Ramos, B., Molano, J. C., & Dorado, C. (2023). A contribution to understanding the origin of the Ginebra Gold District mineralizations, Colombia. Earth Sciences *Research Journal, 27*(4), 327-341. https://doi.org/10.15446/esrj.v27n4.102964

ISSN 1794-6190 e-ISSN 2339-3459
https://doi.org/10.15446/esrj.v27n4.102964

1. Introduction

Despite the available petrogenetic and geochronological studies about igneous and metamorphic rocks cropping out on the western flank of the Central Cordillera (McCourt et al., 1984; Aspden & McCourt, 1986; Restrepo & Toussaint, 1988; Nivia, 2001; Villagómez et al., 2011; Leal-Mejía, 2011; Leal-Mejía et al., 2019, Manco; 2020), the current knowledge about mineral occurrences hosted by some of these units is still poor, especially for late Cretaceous age, although they could contribute to the understanding of the geological processes occurred during that time. This is especially true for the Ginebra Gold District, were a discontinuous SSW-NNE trending mineral belt extends for about 8 km long from the La Esperanza-La Selva to the south to El Retiro-Cueva Loca-La Cecilia to the north.

In the Ginebra district, the mineralization style is principally veined being also common to find disseminations, veinlets and stockworks, especially in the El Retiro area, related to strong sericite-pyrite-quartz alteration. At the La Esperanza-La Selva, instead, mineralization is almost exclusively veined, with narrow sericite-chlorite and propylitic alteration haloes. Although some of these mineralized veins has been attributed to an "Intrusion-related" character, genetically related to the Buga Batholith magmatic event (McCourt et al., 1985; Nivia, 2001; Leal-Mejía, 2011; López et al., 2018; Leal-Mejía et al., 2019), non-conclusive evidences, as their clear magmatic origin, have been reported yet.

In this document, we provide new petrographic, fluid inclusion petrography, microthermometric, Raman spectroscopy, stable isotope and $^{40}Ar/^{39}Ar$ data from Ginebra district, in order to contribute to the understanding of the composition, evolution and nature of the hydrothermal fluids responsible for their generation and relate it to the geological processes occurring during their genesis.

Geological Setting

Geological evolution of the western flank of the Central Cordillera and the eastern flank of the Western Cordillera of Colombia has been controversial for many years and not fully understood, although there is a consensus about the role of accretionary onset of oceanic derived rocks against the continental margin of northwest South America during the late Cretaceous (Cediel et al., 2003; Villagómez et al., 2011; Bustamante & Bustamante, 2019) (**Figure 1**). Most of the evidences conducing to this conclusion relates to lithogeochemical and geochronology, showing a clear correlation between basaltic rocks from Ecuador to the south until Aruba, conforming part of the enormous Caribbean Lithospheric Igneous Province (CLIP) (Cediel et al., 2003; Villagómez et al., 2011; Bustamante & Bustamante, 2019; Nivia et al., 2019).

The Ginebra Gold District is located on the western flank of the Colombian Andes Central Cordillera. At this region, the basement consists of Upper Mesozoic oceanic rocks, accreted to the continental margin of South America because of the drift of the Caribbean plate to the E and NE between the Mesozoic and Cenozoic (McCourt, 1984; Aspden & McCourt, 1986; Restrepo & Toussaint, 1988). This area is framed by two major structural features with an approximate NS to N30°E direction, the Guabas-Pradera and Palmira-Buga faults, which are part of the Cauca-Romeral fault system.

The older geological unit corresponds to the Ginebra Ophiolitic Massif (**Figure 2**), name proposed by Espinosa (1984. In McCourt et al., 1985), referring to a N-S block of ultramafic rocks outcropping on the western flank of the Central Cordillera. Nivia (1987. In Ossa, 2006) affirms it is composed mostly by amphibolites produced by metamorphism of micro gabbro and basalt, with superimposed regional metamorphism effects evidenced by the presence of nematoblastic and lepidoblastic textures as well as quartz and amphibole boudins related to dynamic metamorphism. Based on geological mapping, petrography and mineral chemistry, Nivia et al. (2019) divided the Ginebra Ophiolitic Massif in four different units, the Ginebra Ultramafic, the Ginebra Gabbro and Amphibolite, the Ginebra Anfibolite and the Ginebra Basalt.

Nivia et al. (2019) recognized orogenic metamorphism producing amphibole generation from original pyroxene in gabbro of this unit, generated as consequence of fluids migration through these rocks, evidenced by the occurrence of pegmatitic texture amphibole-plagioclase veins and epitaxial actinolite-tremolite growth on pyroxene, representative of a retrograde green schist facies, progressing to an epidote-amphibolite facies this later deformation phase, dated about 90 Ma, is contemporaneous with the emplacement of the first magmatic event of the Buga Batholith.

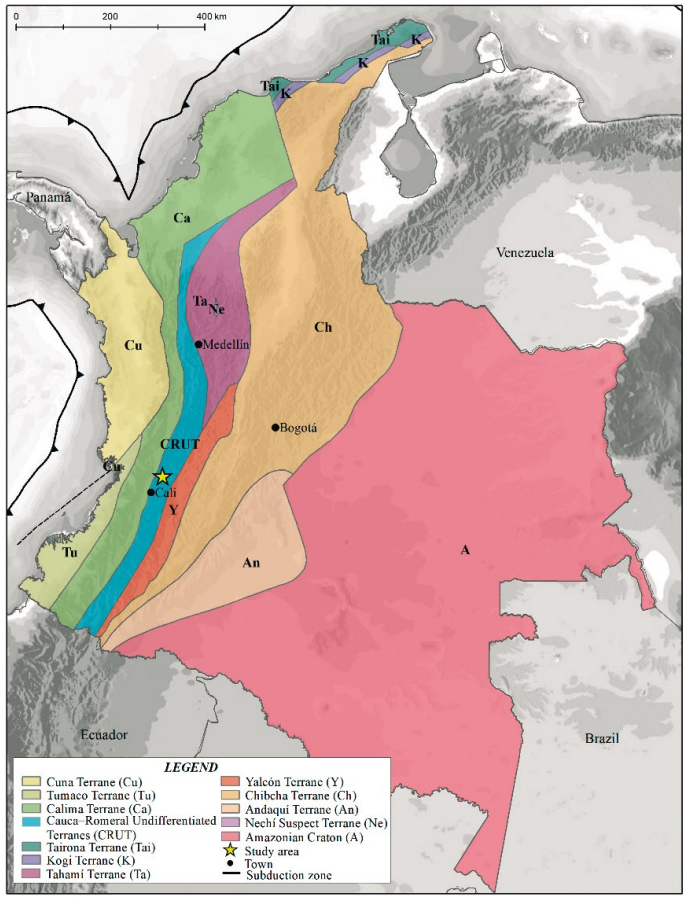

Figure 1. Tectonostratigraphic terranes in Colombia, after Toussaint & Restrepo, (2020). Amazonian Craton (A), Andaquí Terrane (An), Chibcha Terrane (Ch), Yalcón Terrane (Y), Tahamí Terrane (Ta), Kogi Terrane (K), Calima Terrane (Ca), Tumaco Terrane (Tu), Tairona Terrane (Tai), Cuna Terrane (Cu) and Cauca–Romeral Undifferentiated Terranes (CRUT).

^{40}Ar-^{39}Ar analysis indicates a crystallization age of 140.28 ± 3.12 Ma (in clinopyroxene) for a gabbronorite and 90.84 ± 0.78 Ma (in hornblende) for an amphibolite, the later interpreted by Nivia et al. (2019) as the age of reworking due emplacement of the Buga Batholith.

Amaime Formation, originally proposed by McCourt (1984), outcrops along the western flank of the Central Cordillera and consists of a series of massive tholeiitic basalts with pillow lava horizons. The age of this unit is controversial, and although it has been proposed it may be contemporaneous and genetically related with the Ginebra Ophiolitic Massif, being also intruded by the Buga Batholith, averaged ^{40}Ar-^{39}Ar ages 90.6 ±2.5 Ma presented by Kerr et al. (1997; 2002), as well as petrologic and structural evidences provided by Nivia et al. (2019), suggest this unit represents a different plateau-related event.

The Buga Batholith corresponds to a north-south elongated polyphasic calc-alkaline body composed by tonalites, quartz diorites and gabbros, in most areas in faulted contact, after sin-tectonic intrusion in the Ginebra Ophiolitic Massif (Aspden et al., 1987. In Nivia, 2001; Nivia et al., 2019). It presents a general low-K and a mixed ferroan-magnesian nature, with a tholeiitic signature, although the more felsic rocks present a normal calc-alkaline to high calc-alkaline character (Leal-Mejía, 2011; Villagómez, 2010; Leal-Mejía et al., 2019).

Based on lithogeochemical and isotopical evidences, the Buga Batholith in conjunction with other Cretaceous age intrusive bodies as Sabanalarga, Mistrató, Santa Fé and Jejenes, has been proposed as allochthonous, with a more primitive chemical characteristics and being part of the CLIP, accreted to the paleo-autochthonous margin prior to the Andean Orogeny (Leal-Mejía, 2011; Villagómez et al., 2011; Nivia et al., 2019; Leal-Mejía et al., 2019).

Reported radiometric ages for the Buga Batholith includes 113 ± 10 Ma K/Ar age in hornblende (Toussaint et al., 1978), a 99 ± 4 Ma Rb-Sr age in biotite (Brook, 1984) and more recently U-Pb zircon ages between 96 to

111 Ma with a 98.79 ±0.43 Ma Concordia age (Brito et al., 2010), 90.6 ± 1.3 and 92.1 ± 0.8 Ma (Villagómez, 2010; Villagómez et al., 2011).

U-Pb zircon dating reported by Nivia et al. (2019) revealed two age groups, between 90-83 Ma and 70-67 Ma as the result of equal number of magmatic episodes. The later age group is restricted to the northern part of the intrusion and is compatible with the ages (65.4 to 70.61 Ma) for small hypabyssal dacite porphyries intruding to the Ginebra Ophiolithic Massif and the Amaime Formation (Rodríguez-Ramos, 2012; Barrera-Cortes & Molano, 2021) cropping out in La Esperanza, Cominal and Río Flautas sectors in both sides of the Guabas-Pradera fault. Some of these porphyries, especially on the Río Flautas presents deformation evidences due to the Guabas-Pradera fault.

Mineralization in the Ginebra gold district

Mineralization style in the Ginebra district is manly veined, although there is also common to find disseminations, veinlets and stockworks. It is distributed in two main areas, the El Retiro-Cueva Loca-La Cecilia to the north and the La Esperanza-La Selva, about 8 km to the south (**Figure 2**).

At the El Retiro-Cueva Loca-La Cecilia (northern sector), 1 to 35 cm thick sinuous and discontinuous veins with a N20-40°E trend, dipping 30-40° to the SE and NW, being also common to observe stockwork veinlets. Gold bearing structures presents clay and sericite narrow haloes and are hosted by gabbro belonging to the Ginebra Ophiolitic Massif (El Retiro) and by tonalites, granodiorites and diorites of the Buga Batholith (Cueva Loca and La Cecilia). In this area there are also intensely sericite-quartz-carbonate alteration zones (**Figure 3.** A and B), in most cases structurally controlled, affecting to medium grain gabbro, accompanied by quartz-pyrite stockwork veinlets.

At the El Retiro-Cueva Loca-La Cecilia, the veins are composed by mosaic to massive texture quartz and minor calcite with scarce sulfides (**Figure 4.** A and B). At least two different quartz events were identified. The first is composed by subhedral to euhedral massive texture quartz with euhedral and coarse-grained pyrite (**Figure 3.** A and B), while the second is composed by smaller size mosaic quartz crystals associated to calcite, sericite, secondary biotite, chlorite and pyrite as well as galena and chalcopyrite filling fractures in the first pyrite and quartz event (**Figure 4**. C and D).

Molano et al. (2000) and Cervera & Garcés (2005) reports electrum and native gold as blebs in pyrite and quartz as well as fractures filling associated to pyrite, quartz and galena, suggesting two precipitation events.

Conversely, at La Esperanza-La Selva (**Figure 2**), the gold lodes are hosted only by gabbro belonging to the Ginebra Ophiolitic Massif. These structures present a continuous to discontinuous character with a sinuous morphology and a variable thickness between 3 and 90 cm with a main N40-60°W trend dipping 20 to 30° to the NE (**Figure 3.** C, D and E). Only narrow, poorly developed clay to sericite-chlorite alteration halo is observed. Pyrite, chalcopyrite and galena content is a very low in a 97:3 proportion respect to quartz, although locally at the La Selva, about 15% of these sulfides have been identified.

As at El Retiro-Cueva Loca-La Cecilia, two different quartz events were observed at the La Esperanza-La Selva. The first characterizes by subhedral to euhedral coarse grain quartz crystals while the second is composed by smaller size anhedral and mosaic texture crystals. Coarse grain pyrite crystals accompany the quartz of the first generation with small gold blebs embedded in both minerals (**Figure 4**. E).

The second mineralization event is composed by smaller pyrite crystals, associated with minor galena and chalcopyrite filling fractures in the first pyrite and quartz generation. Small grain gold blebs in galena were observed (**Figure 4**. F). Very thin molybdenite veinlets crosscutting the quartz veins as a latest event.

Our petrographic descriptions are in agreement with Molano et al. (2000) who describes two gold events in this area, the first related to pyrite and quartz and the second with chalcopyrite and galena.

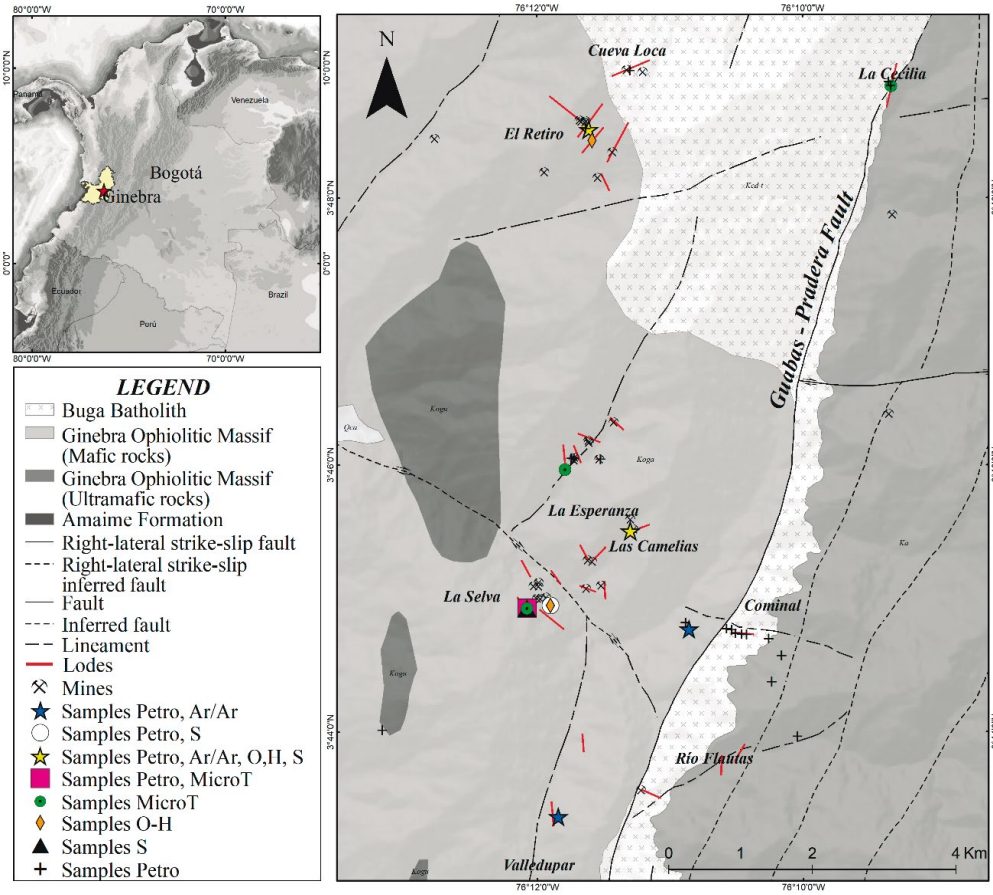

Figure 2. Geological Map of Ginebra Massif (Rodríguez-Ramos, 2012). Modified from Nivia (2001).

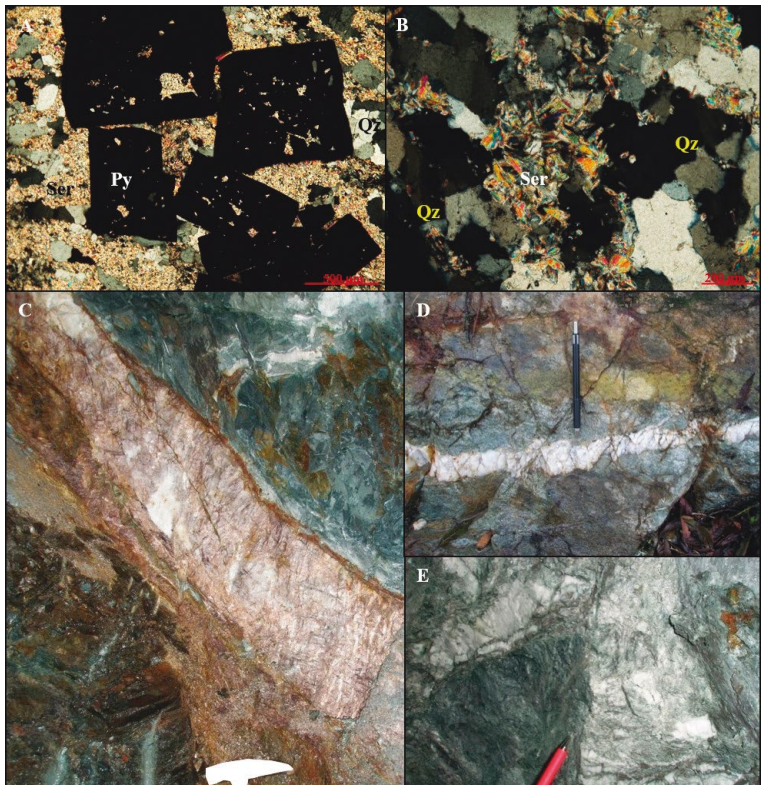

Figure 3. Hydrothermal alteration and vein morphologies of the Ginebra Gold District. A. and B. Strong pervasive sericite-muscovite (Ser) hydrothermal alteration. C, D and E. Sinuous deformed milky quartz veins hosted by the Ginebra Ophiolitic Massif.

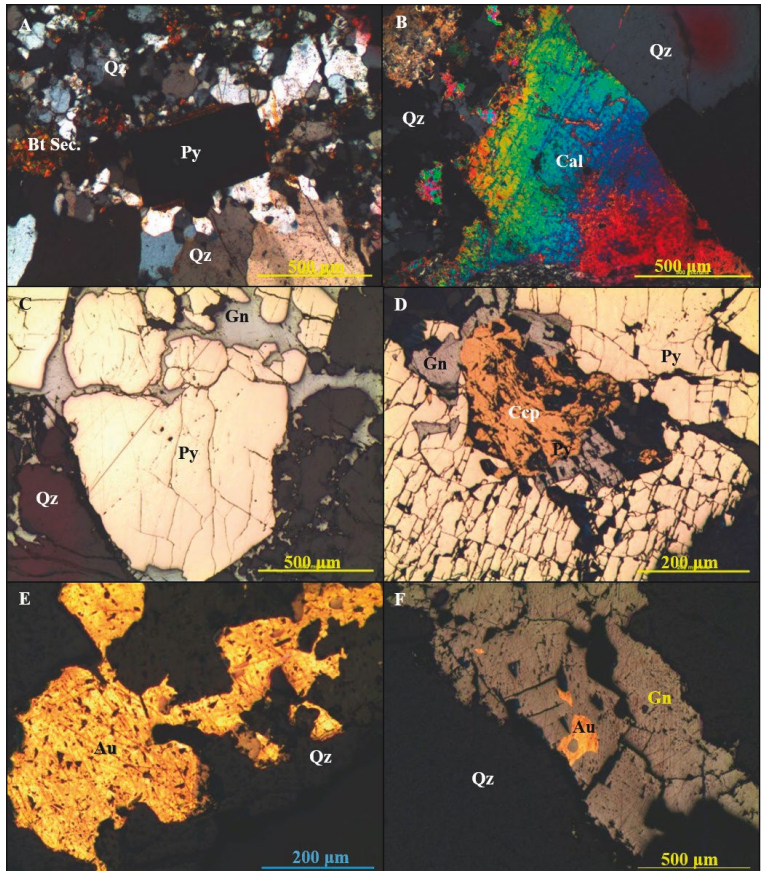

Figure 4. Mineralogy and textural relationships in the Ginebra Gold District. A. Massive and mosaic texture quartz (Qz) crystals associated with euhedral pyrite (Py). B. Euhedral calcite associated with massive quartz (Qz) note a later mosaic texture quartz generation. C. Galena filling fractures in pyrite (Py) crystals associated with quartz (Qz). D. Galena (Gn) and chalcopyrite (Ccp) filling fractures in pyrite (Py). Gold (Au) included in quartz (Qz). F. Gold bleb (Au) in galena (Gn).

As a result of the petrography, a paragenetic sequence for the gold bearing veins and disseminations in the El Retiro-Cueva Loca-La Cecilia and the La Esperanza-La Selva areas is given in **figure 5**.

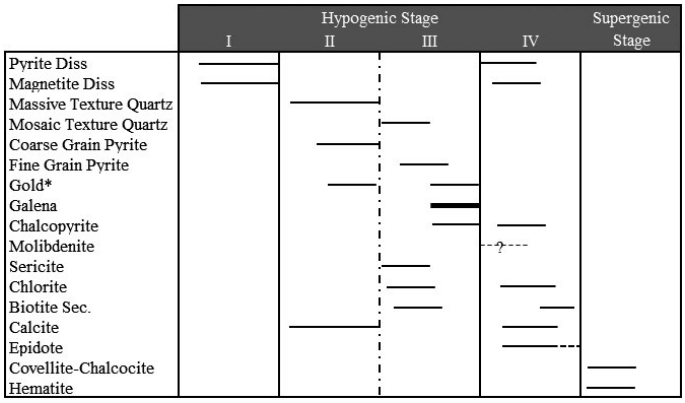

Figure 5. Paragenetic sequence for the vein lodes of the Ginebra Gold District.

Analytical methods

Fluid inclusions microthermometry and Raman spectroscopy

A total of 105 representative samples of gold bearing quartz veins, were collected from artisanal underground workings and surface outcrops, from the La Cecilia to the north to the La Esperanza and the La Selva to the south in the Ginebra district. Five of these samples were selected for fluid inclusions microthermometry and Raman analysis.

Double polished, 120 µm thick, thin sections from quartz samples were prepared by us and analyzed under the microscope. The microthermometric measurements for fifty-nine (59) fluid inclusions were carried out on a Linkham THSM 600 heating-freezing stage and an Olympus BX41 petrographic microscope in the microscopy and microthermometry Laboratory of the National University of Colombia in Bogota. The measuring range between -196ºC and + 600ºC. The accuracy of the equipment was estimated at +1ºC to the lowest temperature and +4.7ºC for the highest. The stage was calibrated measuring two standards of synthetic inclusions from the University of Leoben´s Fluid Inclusions Laboratory, containing H_2O (final ice melting temperature: 0ºC; homogenization temperature: 374.1ºC), and CO_2 (CO_2 melting temperature: -56.6ºC).

Fluid inclusion petrography was performed using the principles given by Roedder (1984) and based on the concept of Fluid Inclusion Assemblage (FIA), which brings together a group of fluid inclusions trapped at the same time (Goldstein, 2003). The FIA methods were determined based on the assumptions given by Roedder (1984) for the recognition of primary, pseudosecondary and secondary fluid inclusions, using the number of phases, their proportions at ambient temperature (25ºC) and the spectroscopic data for the recognition of primary pseudo-secondary and secondary inclusions.

Six phase changes in the fluid inclusions were recorded during cooling/heating routines: (1) CO_2 melting temperature ($TmCO_2$), (2) eutectic temperature (Te), (3) final ice melting temperature (TmIce), (4) clathrates melting temperature (TmCLAT), (5) CO_2 homogenization temperature ($ThCO_2$) and (6) total homogenization temperature (Th). Salinity determination was made using the Q2 and ICE programs from CLATHRATES package (Bakker, 1997; Bakker & Brown, 2003), by using Peng & Robinson (1976) and Duan et al. (1992) state equations according to the characteristics of each type of inclusion.

The salinity, density and molar volume for the most of the acuo-carbonic fluid inclusions, were modeled on the Q2 program (Bakker, 1997; Bakker & Brown, 2003), because the carbonic phase homogenization occurred in all the cases in one of the quadruple system points. The calculations used the state equation of Peng & Robinson (1976) and the composition of the non-aqueous phases from the Raman spectroscopy (XCO2= 0.91, XN2=0.09).

In contrast, for those of the acuo-carbonic fluid inclusions lacking immiscible carbonic phases, the salinity, density and molar volume were calculated using the ICE program from the CLATHRATES package (Bakker, 1997; Bakker & Brown, 2003), using the state equation from Duan et al. (1992).

Additionally, Raman analyses were carried out in the vapor phase of the inclusions. These measurements were performed at laboratories of the United States Geological Survey (USGS) and the facilities of the Technological Development Center of the Colombian Emerald (CDTEC) located in Bogotá, using a Nicolet Almega equipment, which uses a laser with a wavelength of 532 nm. Deviations used to the identification of the molecular species in the fluid inclusions were the established by Burke (2001) and Frezzotti et al. (2012).

Oxygen, deuterium and sulfur stable isotopes

From petrographic determinations and using x-ray diffraction analysis on disoriented and oriented laminae using an ethyl-glycol routine, to confirm the abundance and a high crystallinity of the sericite-muscovite, there were selected three samples from hydrothermal alteration halo from mineralized quartz veins: (1) from the La Reserva mine in La Selva area, (1) stockwork quartz-sericite-pyrite veinlets in intensely hydrothermally altered gabbro from El Retiro mine, El Retiro-Cueva Loca-La Cecilia area, and (1) hydrothermal sericite affecting to a dacite porphyry from El Castillo zone, to the south of the district. For these samples, δ18O and δD compositions were acquired in a SIRA-II –DualInlet mass spectrometer in the Salamanca University (Spain). The δ18O and δD isotopic composition of the hydrothermal fluid in each simple was calculated in equilibrium with muscovite at 300ºC, concordant with the total homogenization temperatures from fluid inclusions analysis, using the fractionation coefficients proposed by Zheng (1993) and Suzuoki & Epstein (1976). The δ18O and δD results are standardized to the VSMOW.

For the sulfur isotope determinations, three mineralized quartz veins samples from La Reserva, Cascabel and Las Camelias mines, from La Esperanza-La Selva area and one sample from stockwork quartz-sericite-pyrite veinlets in intensely hydrothermally altered gabbro from El Retiro mine were selected. Isotopic values were measured in a Thermoquest-Finnigan DELTA PLUS XL mass spectrometer in the United States Geological Survey (USGS) and the results were standardized to the Devil Canyon Troilite (DCT).

The hydrothermal fluid composition for 250ºC, in terms of $\delta^{34}S_{H2S}$, was calculated using the sulfur enrichment factors proposed by Sakai (1968), Kajiwara & Krouse (1971) and Czamanske & Rye (1974).

Samples were crushed and sieved, choosing the 125 - 250 µm fraction. This granulometric fraction was then washed with de-ionized water and dried at low temperature to be later separated using a Frantz magnetic separator using 0.4, 0.6, 1 and 1.5 A. The final sericite and pyrite, galena and chalcopyrite fraction were hand-picked to obtain about 50 mg for each sample. In the case of the sulfides, there was verified a clean and unaltered aspect.

The δ18O and δD isotopic composition of the hydrothermal fluid in each sample was calculated in equilibrium with muscovite at 300ºC, concordant with the total homogenization temperatures from fluid inclusions analysis, using the fractionation coefficients proposed by Zheng (1993) and Suzuoki & Epstein (1976). The δ18O and δD results are standardized to the VSMOW.

$^{40}Ar/^{39}Ar$ dating

To have a better understanding of the age of the Ginebra Ophiolitic Masiff, one of the two main host unit of the gold lodes in the Ginebra District and its temporal association with the mineralization in the studied area, two un-weathered and hydrothermally unaltered or only very weakly altered plagioclase hornblendite and hornblende gabbro samples, from Cominal-El Jardín and Valledupar-Flautas areas, were selected for dating.

Also, two intensely hydrothermally altered samples, from a quartz-sericite-pyrite stockwork veinlet zone in El Retiro mine and from the sericite-chlorite alteration halo of a mineralized vein from Las Camelias mine from La Esperanza-La Selva area were analyzed. The presence of absence of hydrothermal alteration and weathering was confirmed petrographically.

Mineral separates of hornblende, sericite and chlorite were prepared from the 0.5 to 0.25 mm sieved fraction from jaw-crushed samples, which were washed with de-ionized water, dried and re-sieved. A hand magnet was used to remove magnetite grains and then the samples were magnetically separated using a Frantz magnetic separator. Pure hornblende (~100 mg), chlorite (~60 mg) and sericite (~60 mg) where then hand-picked under a binocular microscope.

The samples were analyzed in the Oregon State University Argon Geochronology Laboratory where they were packaged, irradiated and analyzed for their Ar isotope compositions in a Thermo Scientific ARGUS VI multi-collector noble gas mass spectrometer.

$^{40}Ar/^{39}Ar$ dating results are presented as a step-heating spectra containing the calculated plateau and inverse isochron ages. For most of the analyzed samples, the calculated plateau age was considered the preferred.

Fluid inclusions microthermometry and Raman Spectroscopy results

Fluid inclusions petrography

Based on petrography, four different fluid inclusions FIA were identified in El Retiro-Cueva Loca-La Cecilia and La Esperanza-La Selva localities, presenting different phases at room temperature (22ºC) and different stages (**Table 1**). All the analyzed fluid inclusions are hosted in coarse size quartz crystals (200 µm – 1 mm) related to the first mineralization event identified in petrography (**Figure 5)**.

Table 1. Types of fluid inclusions identified in Ginebra Gold District.

FIA	Host mineral	Phases	Composition*	Origin	L/V	Form
I	Qz	Lcar+Vcar/ Laq	$(CO_2+N_2)_V + (CO_2+H_2O)_L + (H_2O)_L$	Primary	0.12 -0.52	Regular, irregular, ovoid
II	Qz	L+V	$(CO_2 (?)+ N_2 (?))_V / (H_2O)_L$	Pseudo-secondary	0.12 -0.49	Ovoid, rounded, regular
III	Qz	L+V	$H_2O_V + H_2O_L$	Secondary	0.97 - 0.71	Ovoid, regular
IV	Qz	L	H_2O_L	Secondary	-	Ovoid

Vapor (V), liquid (L), quartz (Qz), after Raman (*).

FIA I acuo-carbonic fluid inclusions are were observed as isolated and randomly distributed in intragranular quartz crystals, therefore were classified as primary to pseudo-secondary. At room temperature (20ºC), these fluid inclusions exhibit three phases (carbonic vapour, carbonic liquid and acuous liquid), with variable phase ratios (Lcar+Vcar/Laq) between 0.12 and 0.52. Presents regular to very irregular and ovoid shapes, and a size ranging from 4.7 to 19.9 µm (**Figure 6.** A and B).

FIA II inclusions are not frequent, but are present in all the analyzed sectors, coexisting with FIA I inclusions. They are pseudo-secondary in origin, aligned along sealed fractures, which do not completely cross the crystals containing them **(Figure 6.** C). They are biphasic, liquid-rich inclusions, with a phase relationship (V/L) between 0.12 and 0.49, with ovoid, rounded and regular shapes, and with sizes between 3 and 11 µm.

The FIA III inclusions are the most common inclusions observed in the studied plates, and were identified as secondary inclusions align as trails, along fractures crossing boundaries grains. They are two phases, liquid-rich fluid inclusions, with a proportion of the liquid phase between 0.97 and 0.71, with usually ovoid and regular shapes, and minuscule sizes (3.7 and 5.3 µm) (**Figure 6.** D). Giving their small size, there was not possible to analyze their phase changes.

The FIA IV inclusions are relatively frequent, have a secondary origin and are characterized by only having a liquid phase at room temperature (**Figure 6.** D).

Microthermometric results

Microthermometric results of the most significant recorded phase changes for the FIA I and II fluid inclusions are summarized here because of their primary and pseudo-secondary origins, providing information about the fluids related to the gold genesis in the Ginebra district. Although FIA III fluid inclusions may provide useful information about the evolution of the system, their small size made analysis impossible.

During the heating/freezing routines, the melting temperatures of the carbonic phase ($TmCO_2$) for the FIA I fluid inclusions occurred between -60 to -56ºC (**Table 2; Figure 7**), generally below the triple point of pure CO_2, indicative for the existence of other non-aqueous species within the carbonic phase. The partial homogenization of the carbonic phases ($ThCO_2$) occurred by the disappearing of the CO_2 vapor (Lcar + Vcar = Lcar) but also to vapor CO_2 (Lcar + Vcar = Vcar), suggesting different densities between fluid inclusions within the same type in paragenesis. This phase change occurred between 11.3 to 30.9ºC.

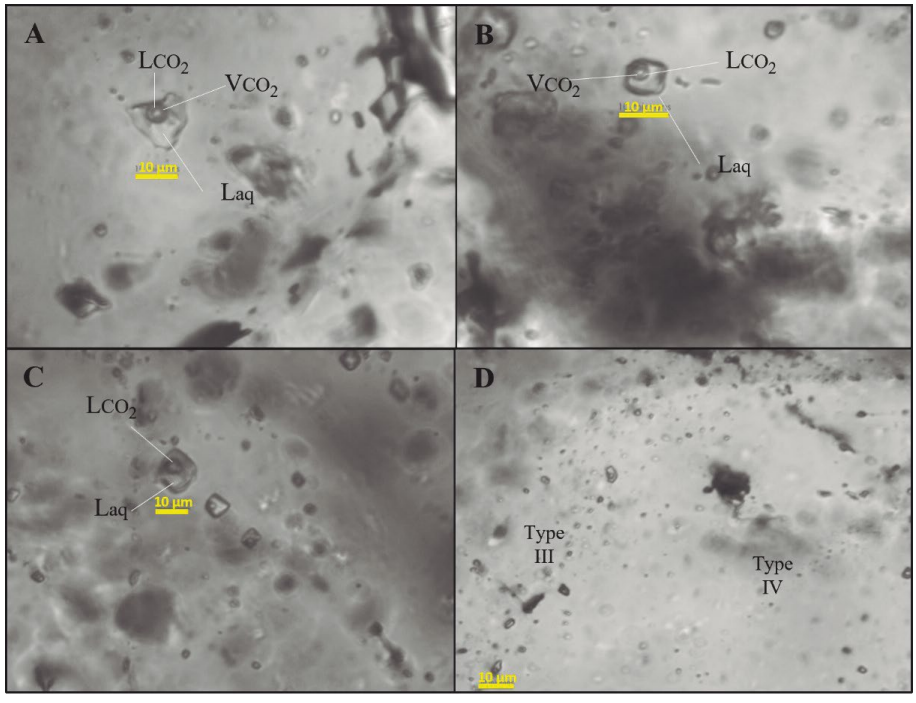

Figure 6. A and B. FIA I primary inclusions, with three phases at room temperature. C. Aligned FIA II pseudo-secondary inclusions, biphasic compositions and which are liquid-rich. D. Aligned FIA III and IV secondary inclusions, biphasic inclusions and monophasic inclusions, respectively.

Although, from the petrography analysis, the fluid inclusions with evidences of leaking, necking down or decrepitation were discarded for the microthermometry, most of the FIA I inclusions decrepitated before their full homogenization, at temperatures from 239 to 309.6ºC, as a result of an internal overpressure when the temperature increased during the heating routines. Total homogenization temperatures for those inclusions which not decrepitated range from 237.4 to 301.6ºC (**Table 2; Figure 7)**.

Because of their scarcity, only few microthermometric results were obtained for FIA II inclusions. In all the analyzed samples, there were recognized four phase changes during the microthermometric routines. The final ice melting temperatures (TmIce) range between -0.8 and -8.1ºC. Clathrates were identified in this fluid inclusions type, whose melting temperature ranges between 4.2 and 7.6ºC. Type II inclusions homogenized to liquid from 257.7 to 305.5ºC.

Table 2. Microthermometry results for FIA I and II fluid inclusions from the Ginebra Gold District.

Zone of study	$TmCO_2$ (T°)	TmCLAT (T°)	$ThCO_2$ (T°)	Th (T°)	Tdec (T°)	Salinity wt% NaCl equiv.
La Cecilia FIA I	-59.5°C to -56°C	7.6°C - 9.3°C	25.9°C - 30.9°C	239.5°C - 263°C	239°C - 271°C	0.75 - 4.0
La Cecilia FIA II	-	7.6°C	-	257.7°C	-	4.4
La Esperanza FIA I	-58°C	6.4°C - 7°C	11.3°C - 23.4°C	-	265.4°C - 272°C	5.12 - 6.22
La Selva FIA I	-60°C to -53.7°C	6.5°C - 9°C	15.5°C - 29.6°C	237.4°C - 301.6°C	255.4°C - 309.6°C	1.33 - 6.06
La Selva FIA II	-57.1°C to - 56.4°C	0.5°C - 6.1°C	-	226.9°C - 305.5°C	246.5°C	4,6 - 9,3

CO_2 melting temperature ($TmCO_2$), clathrates melting temperature (TmCLAT), CO_2 homogenization temperature ($ThCO_2$), homogenization temperature (Th), decrepitation temperature (Tdec).

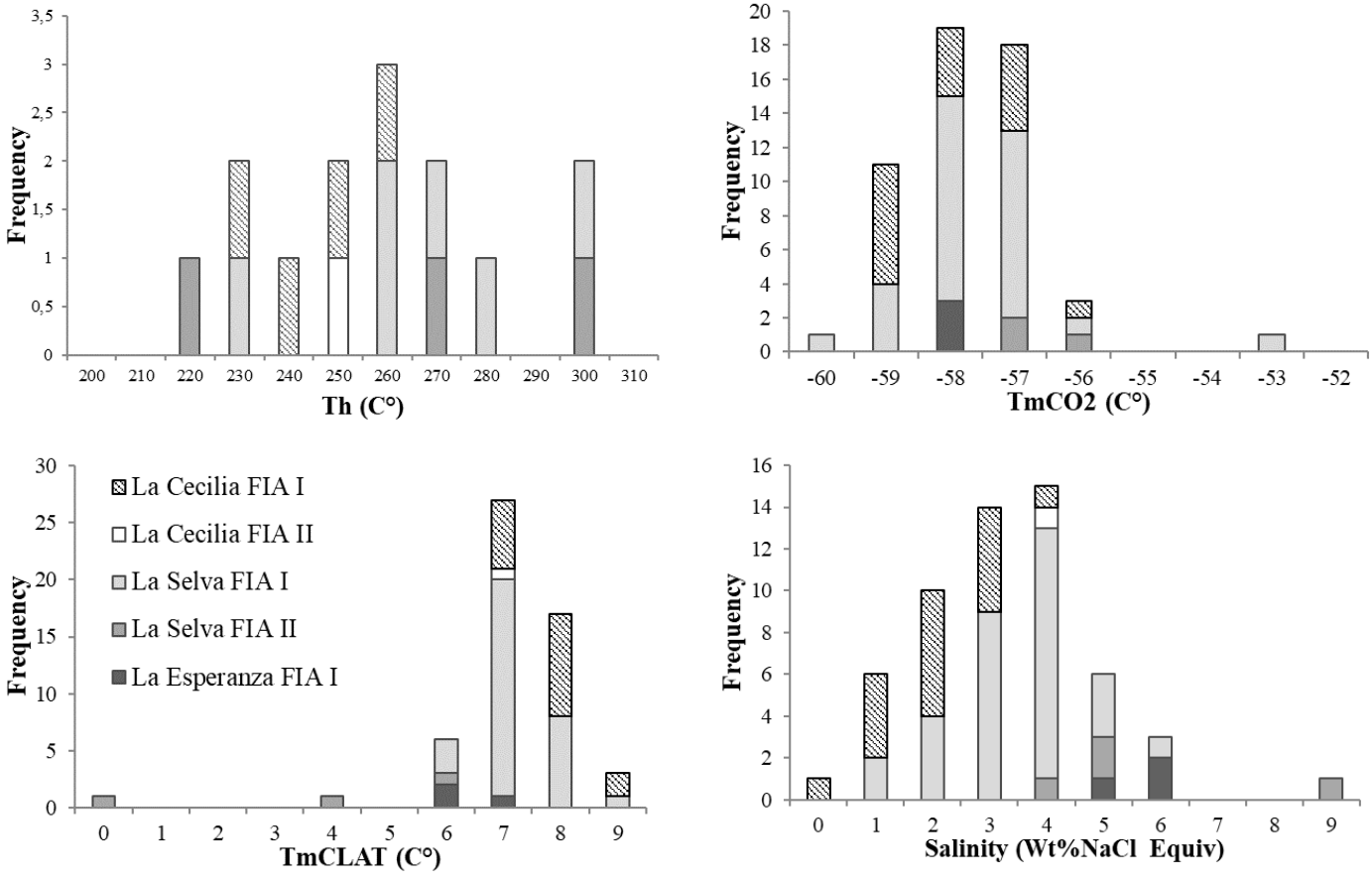

Figure 7. Frequency histograms for CO_2, clathrates and total homogenization temperatures as well for calculated salinity from fluid inclusions in the Ginebra Gold District.

Raman spectroscopy

Due to the small size of the fluid inclusions in Ginebra gold mineralization, was difficult to run the spectroscopic analysis. However, it was possible to carry out the determination of the volatile species from FIA I inclusions, confirming the presence of CO_2 and the existence of N_2, responsible for the gas hydrates (clathrates) formation during the cooling routines (**Figure 8**). This is consistent with the measured melting temperatures of CO_2.

The quantity of CO_2 and N_2 is variable, although the former is the dominant species in the measured inclusions, with relative proportions between 91 and 100%, while for N_2, the amounts are usually small, from nonexistent to about 9%, in some cases reaching 22%.

Mineralizing fluids composition

FIA I inclusions presents moderate to low salinities, from 0.75 to 6.22 wt% NaCl equiv., being slightly higher in the La Esperanza zone comparing with the La Cecilia and the La Selva areas. Density varies from 0.92 to 0.99 g/cc while the molar volume ranges from 19.0 to 24.23 cc/mol.

Like FIA I inclusions, FIA II presents low to moderate salinities from 4.4 to 9.34 wt% NaCl equiv., being slightly higher in La Selva area, compared to La Cecilia zone. The liquid phase total density varies from 0.89 to 0.90 g/cc and a molar volume from 21.04 to 23.67 cc/mol.

Stable isotopes results

Oxygen and deuterium isotopes

The three intensely sericitic altered analyzed samples presents a δ^{18}VSMOW (Vienna Standard Mean Ocean Water) composition ranging from +8.6 to +11.2‰ and δD VSMOW from 50.8 to -74.6‰ (**Table 3**). Using the fractionation coefficients proposed by Zheng (1993) and Suzuoki & Epstein (1976) at 300ºC, compatible with the total homogenization temperatures from the fluid inclusions, the hydrothermal fluid responsible for this alteration have a δ^{18}VSMOW isotopic values ranging from +4.14 to +9.73‰ and δD VSMOW values from -3.96 to -28.93‰ (**Figure 9**).

Sulfur isotopes

Pyrite, galena, chalcopyrite separates returned δ^{34}S values from +1.1 to +1.4 ‰ for the galena and a wider range for pyrite, between -8.2 to +4.8 ‰. One chalcopyrite sample returned +2.4 ‰ (**Table 4; Figure 10**).

Using the sulfur enrichment factors proposed by Sakai (1968), Kajiwara & Krouse (1971) and Czamanske & Rye (1974), the hydrothermal fluid composition for 250°C, in terms of $\delta^{34}S_{H2S}$, was calculated from -8.5 and 5.3‰.

From the paragenetic galena-chalcopyrite mineral pair, from vein mineralization at La Selva area, there was calculated a 364.18ºC as the isotopic fractionation temperature using the coefficient values proposed by Kajiwara & Krouse (1971).

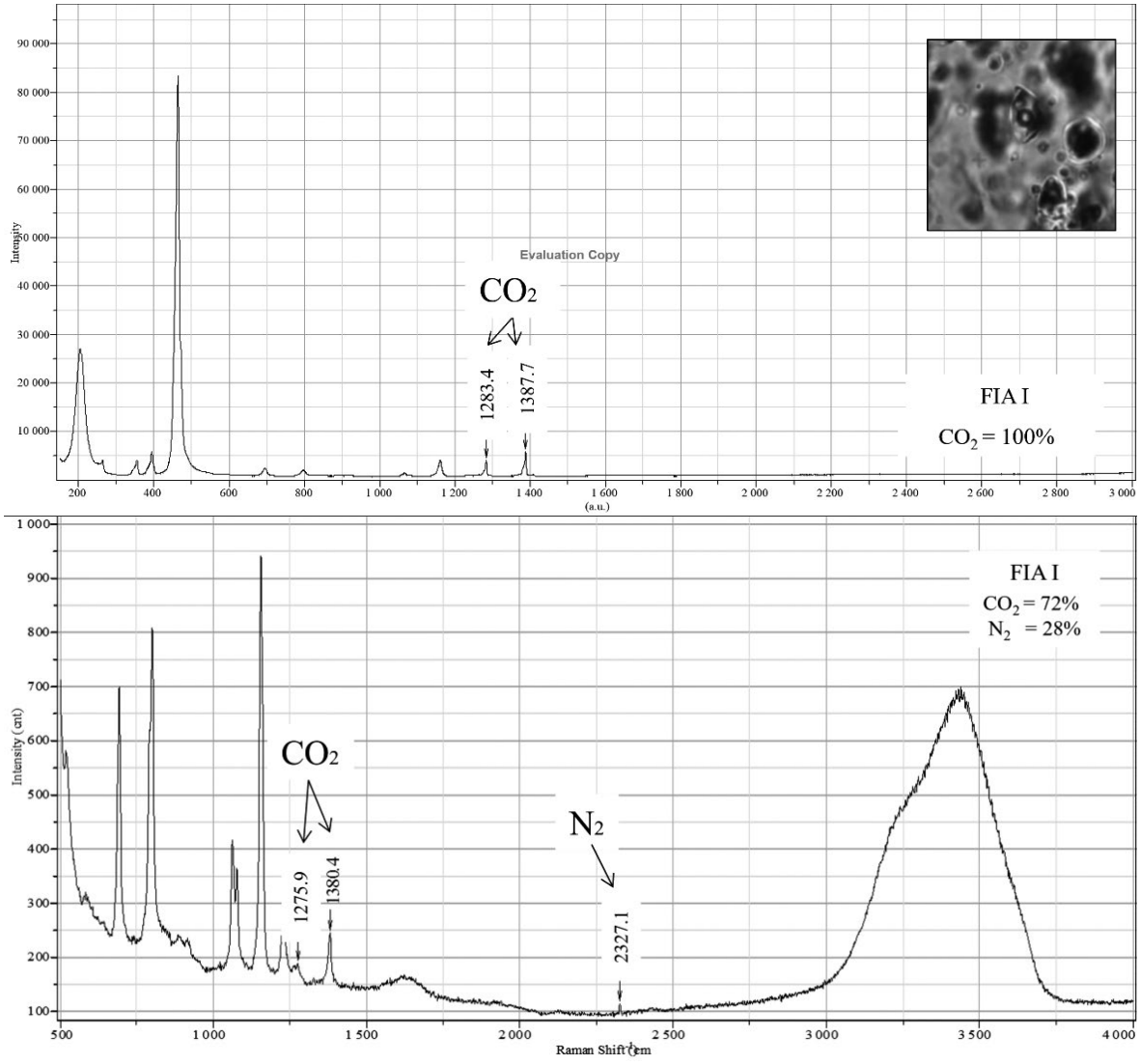

Figure 8. Raman spectra of FIA I inclusions, where the presence of CO_2 and N_2 in the vapor phase is identified.

Table 3. Deuterium and oxygen isotopic results from hydrothermal sericite. Results are standardized respect to VSMOW.

Sample	Mineral	$\delta^{18}O$ VSMOW	δD VSMOW	% H_2O	$\delta^{18}O$ VSMOW (H_2O)	δD VSMOW (H_2O)
1170	Sericite	8.6‰	-64.1‰	4,3	7.14‰	-17.99‰
1452	Sericite	9.6‰	-74.6‰	0,2	8.14‰	-28.93‰
1499	Sericite	11.2‰	-50.8‰	7,6	9.73‰	-3.96‰

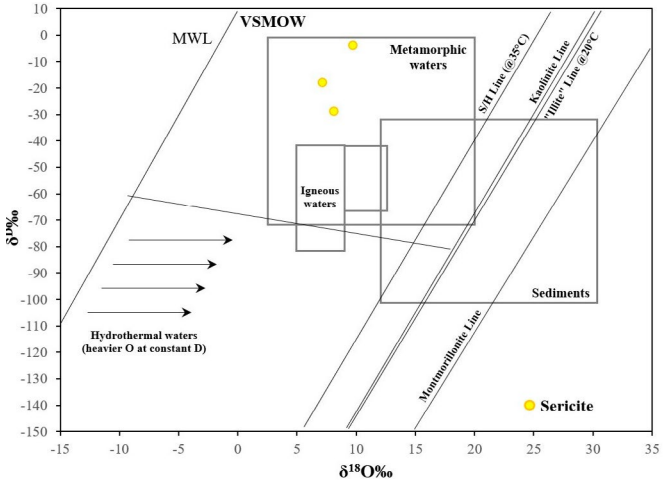

Figure 9. δ18O y δD isotopic composition for the hydrothermal fluid responsible for the hydrothermal sericite related to the Ginebra Gold District mineralization. Modified from Sheppard, 1986.

Table 4. Sulfur isotope composition of sulfide samples from the Ginebra Gold District.

Sample	Location	Mineral	$\delta^{34}S$ CDT‰
1169	La Selva	Chalcopyrite	2.4
1169	La Selva	Galena	1.1
1169	La Selva	Galena	1.4
1495	Las Camelias	Galena	1.2
1187	La Selva	Pyrite	-8.2
1495	Las Camelias	Pyrite	3.5
1170	El Retiro	Pyrite	4.8

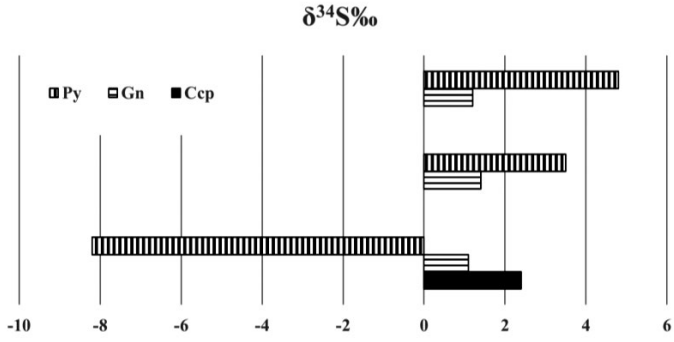

Figure 10. Sulfur isotope results in sulfides from the Ginebra Gold District. Pyrite (Py), Galena (Gn), Chalcopyrite (Ccp).

40Ar/39Ar Dating Results

Two samples from mineralized veins and stockwork veinlets, one from El Retiro mine and the other from Las Camelias mine at La Esperanza-La Selva were select for $^{40}Ar/^{39}Ar$ dating to constrain the hydrothermal event, responsible for Ginebra gold district mineralization.

Two additional samples from a hornblendic gabbro and a plagioclase rich hornblendite belonging to the Ginebra Ophiolithic Massif, close to its eastern border, cropping out in the Cominal-El Jardín and Valledupar-Flautas areas were also analyzed. Results are summarized in **table 5** and illustrated in **figure 11**.

Unaltered medium grain hornblendic gabbro, composed by euhedral hornblende and plagioclase crystals with minor quartz and interstitial fine grain magnetite and ilmenite crystals. Hornblende yielded a weighted plateau age (>97% of the gas release) and inverse isochron overlapping within uncertainty, being the 96.84 ± 2.14 Ma (MSWD = 0.3) plateau age preferred (Early Cretaceous).

Coarse grain plagioclase horblendite composed dominantly by euhedral hornblende and plagioclase crystals with interstitial magnetite, rutile and small pyrite crystals, it presents very weak epidote-carbonate-chlorite-sericite alteration. Hornblende yielded a weighed plateau and inverse isochron overlapping ages within uncertainty, being preferred the 123.57 ± 2.83 Ma (MSWD = 1.07) plateau age (Early Cretaceous).

El Retiro mine from an intensely sericitized and mineralized zone crosscut by thin quartz-pyrite veinlets, in a medium grain gabbro belonging to the Ginebra Ophiolitic Complex. In petrography, there were observed euhedral coarse grain pyrite crystals accompanying to anhedral-mosaic texture quartz crystals and fine-grained sericite. The sample yielded a slightly discordant age spectrum but including a well-defined plateau segment representing 89% of the gas release. The calculated plateau and inverse isochron overlap within uncertainty, and the former age, 67.81 ± 0.87 Ma (MSWD = 1.82), is the preferred age (Late Cretaceous).

Finally, the sample from the Las Camelias mine corresponds to the alteration halo of a 30 cm thick quartz-pyrite-galena-chalcopyrite-sericite-chlorite vein. Chlorite yielded a slightly discordant age spectrum but including a well-defined plateau segment representing 72% of the gas release. The calculated plateau and inverse isochron overlap within uncertainty, being the former age, 65.50 ± 0.84 Ma (MSWD = 0.68), the preferred age (Late Cretaceous).

Discussion

Hydrothermal fluid composition, mixing or effervescence mechanisms, pH, oxidation state, trapping temperature and pressure conditions

The microthermometric and Raman spectroscopy measures of ore-related fluid inclusions from the Ginebra Gold District mineralizations, revealed the hydrothermal fluid presented a relatively simple and only slightly variable acuo-carbonic composition in all the different areas along the mineralized trend. Gold mineralization was produced by a low to moderate salinity CO_2-rich hydrothermal fluid with N_2 minor amounts.

The existence of fluid inclusions of the same assemblage (FIA) with slightly different phase proportions but homogenizing by the vapor disappearing in all the cases, in a restricted temperature range suggests a boiling process may rule out. In contrast, a lineal tendency in the salinity values in restricted homogenization temperatures, observed for FIA I and FIA II (**Figure 12**) may be interpreted as the result of an isothermal fluid mixing process (Wilkinson, 2001).

Homogenization temperatures can be used to calculate trapping conditions at the time the fluid inclusions genesis. However, it is important to remember the total homogenization temperatures represents only a minimum estimate for trapping temperatures and pressures, except when clear evidences of fluid immiscibility exist (Roedder & Bodnar, 1980). In Ginebra Gold District, calculated isochores for FIA I indicate a pressure ranging from 307 to 423 MPa, corresponding to a trapping depth from 11.2 to 15.5 km, assuming a 2.78 g/m^3 density for the crust.

Table 5. $^{40}Ar/^{39}Ar$ Ages for samples from the Ginebra Gold District.

Sample No.	Latitude	Longitude	Location	Petrographic notes	Mineral separated (wt.)	Classification	Condition	$^{40}Ar/^{39}Ar$ plateau age (Ma ± 2 σ) (% ^{39}Ar release isochron age)	$^{40}Ar/^{39}Ar$ isochron age (Ma ± 2 σ)
1482	3.7433	-76.1776	Cominal-El Jardín	Medium-grained Plag(<1mm)-Hbl with interstitial Mag	Hornblende (101.1 mg)	Plagioclase hornblendite	Weakly hydrothermally altered	123.57 ± 2.83 (96.85%)	112.66 ± 10.80 (MSWD=1.07)
1465	3.7198	-76.1940	Valledupar-Flautas	Medium-grained Plag(<1mm)-Hbl with interstitial Mag-Ilm	Hornblende (106.5 mg)	Hornblendic gabbro	Fresh	96.84 ± 2.14 (97.5%)	97.40 ± 6.10 (MSWD=0.3)
1170	3.8057	-76.1901	El Retiro mine	Fine grained sericite accompanying mosaic texture quartz and coarse euhedral pyrite	Sericite (59 mg)	Stockwork veining zone	Intensely hydrothermally altered	67.81 ± 0.87 (89%)	67.73 ± 0.88 (MSWD=1.82)
1495	3.7555	-76.1849	Las Camelias mine	Qz-Py-Gn-Ccp vein with fine grain sericite and medium grain chlorite halo	Chlorite (61 mg)	Quartz vein	Intensely hydrothermally altered	65.50 ± 0.84 (72%)	66.38 ± 1.24 (MSWD=0.68)

Plagioclase (Plag), Hornblende (Hbl), Magnetite (Mag), Ilmenite (Ilm), Quartz (Qz), Pyrite (Py), Galena (Gn), Chalcopyrite (Ccp).

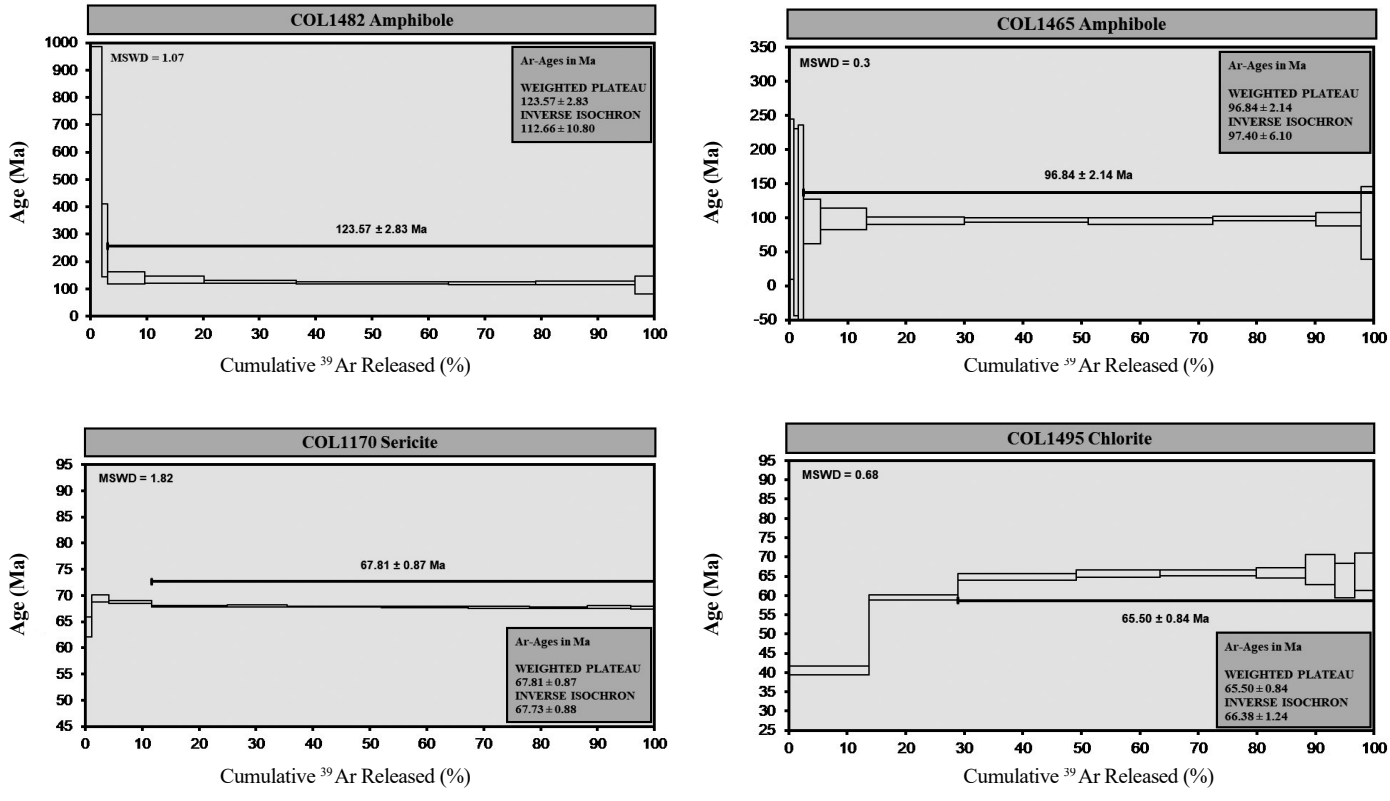

Figure 11. $^{40}Ar/^{39}Ar$ age spectra for samples from the Ginebra Ophiolitic Massif and for stockwork veinlets and gold bearing veins hydrothermal haloes in the Ginebra Gold District.

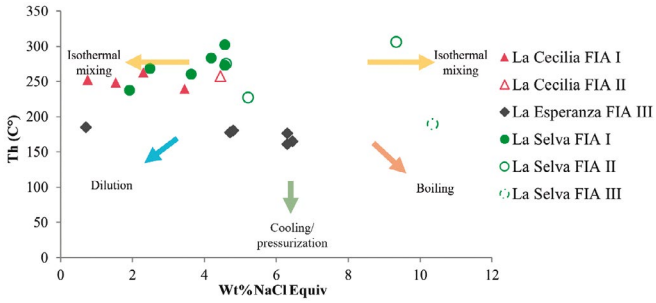

Figure 12. Th vs. salinity diagram (wt% NaCl Equiv.) for FIA´S I, II and III, where is observed a linear trend of the salinity values in a restricted range of homogenization temperatures for FIA I and II, while for the FIA III, salinity is on a range of higher temperature. The tendency of FIA´S I and II is interpreted as a product of an isothermal fluid mixture process. Modified from Wilkinson, 2001.

Because non conclusive evidences of fluid immiscibility and the un-existence of other geo-thermobarometers for the Ginebra Gold District, the calculated P-T trapping conditions represents only minimum values and has to be viewed as the only available information about the depth to which the ores may have been formed.

The alteration mineral assemblage (sericite – muscovite + carbonate ±epidote) in Ginebra Gold District suggests a near-neutral pH conditions (Phillips & Groves, 1983) for the hydrothermal fluid.

Meanwhile, the CO_2 and variable N_2 contents identified in the microthermometry and Raman spectroscopy indicates a relatively reduced character for the hydrothermal fluids, coherent with the sulfides mineralogy, abundant pyrite and absence of arsenopyrite.

Under this aforementioned condition, the oxygen fugacity (fO_2), calculated for the FIA I, using a 300 MPa pressure and a 5.5 pH, ranges from 10^{-31} to 10^{-38} bar (**Figure 13**), confirming a reduced condition for the hydrothermal fluid, which is compatible with the sulfide mineralogy.

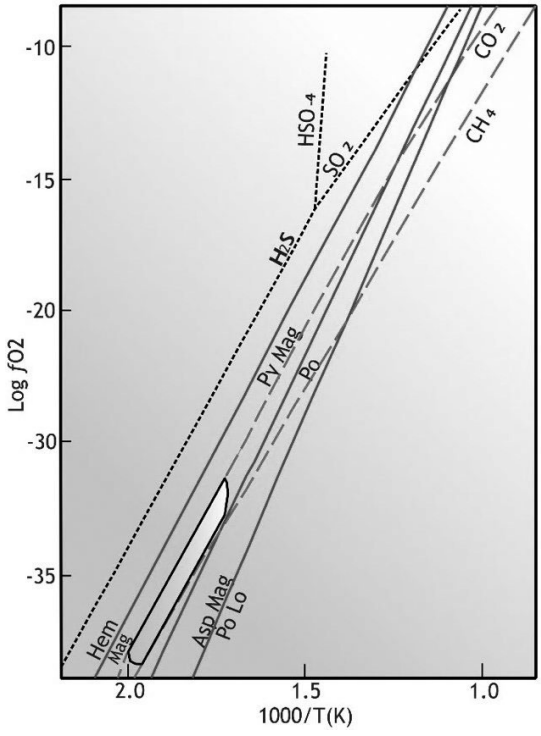

Figure 13. Oxygen fugacity vs temperature diagram for the mineralizing fluids in the Ginebra Gold District mineralization at pH=5.5 and P=300 MPa. Modified from Jia et al., 2000.

Gold transport and deposition mechanisms

Different authors have proposed the gold transport mechanisms in reduced hydrothermal solutions in equilibrium with pyrite/pyrrhotite, containing chlorides and sulfides (Seward, 1973; Seward, 1984; Hayashi & Ohmoto, 1991), in a temperature range between 160 and 350ºC and pH conditions ranging from 1.4 to 9.5. Experimental results and thermodynamic data indicates that in near neutral conditions and a temperature between 250 and 350ºC, as the existing conditions in the Ginebra Gold District, gold is effectively transported only as bi-sulfide to thio-sulfide complexes ($(HAu(HS)_2)^0$, $Au(HS)^-_2$; $AuHS^0$, $AuHS(H_2S_3)^0$) (Seward, 1973; Shenberger & Barnes, 1989; Stefánsson & Seward, 2004). This process neglects the chlorine complexes as effective ligands for gold, except if the fluid is low in H_2S, rich in chloride and the pH is less than 4.5 (Hayashi & Ohmoto, 1991).

The reduced, low salinity and near-neutral condition of the Ginebra Gold District hydrothermal fluid, as well as the close association between gold and sulfides, suggest that the most probable gold transporting mechanism was as bi-sulfide or thio-sulfide complexes.

Several different mechanisms have been proposed for the metal's ligands destabilization in hydrothermal solutions and the correspondent gold precipitation. In general, it has been assumed that any change in the physic-chemical conditions of the hydrothermal fluids may produce their precipitation (Robb, 2005), however, some processes are considered more important, depending not only of the fluid conditions, but of the host rocks and the predominant geological process occurring in the area during the hydrothermal process.

In the case of the bi-sulfide and thio-sulfide complexes, the most important processes invoked for gold deposition includes the phase separation (ebullition or effervescence), as a direct consequence of sudden pressure decrease (Diamond, 1990; Ramboz et al., 1982; Ridley et al., 1996; Sterner & Bodnar, 1984), the pH and oxidation changes due to fluid/rock interactions, the H_2S loss in the hydrothermal fluid due to a sulfidation process, reflected as abundant sulfides (mainly pyrite) generation on the host rocks, and fluid mixing (Gebre-Mariam et al., 1993; Groves, 1993).

The coexistence of FIA I and FIA II fluid inclusions in all the analyzed areas, presenting a marked and constant homogenization by the vapor phase disappearing in a restricted temperature range, showing a lineal tendency in salinity changes, indicates a fluid mixing process may be responsible, at least in part, for the destabilization of the bi-sulfide and/or thio-sulfide complexes and the gold deposition from the hydrothermal fluids in the Ginebra Gold District.

Additionally, most of the host rocks in the district correspond to gabbro belonging to the Ginebra Ophiolitic Massif, presenting a high iron content, susceptible for sulfides generation when these rocks interact with hydrothermal solutions and the correspondent H_2S loss. This sulfidation process may also contributed to the bi-sulfide/thio-sulfide complexes destabilization and gold deposition, particularly in El Retiro-Cueva Loca-La Cecilia area, where is frequent to observe a high volume of fine grain disseminated pyrite around veins and stockwork zones.

We propose that the H_2S loss due to sulfidation and fluid mixing were responsible for gold deposition from the hydrothermal solutions in the Ginebra Gold District.

The nature of ore fluids, age and genetic type of the ore deposit

The characteristics of ore fluids in the Ginebra Gold District are compatible with the orogenic and/or intrusion-related gold deposits. In both cases, CO_2-rich low salinity fluids are responsible for gold transport, both are poor in metals and mineral zoning and they present an imprecise spatial and genetic relationship to individual intrusive phases. These are the reasons to the many existent controversies about the assignment of a particular deposit to any of these categories (Sillitoe & Thompson, 1998; Thompson et al., 1999; Groves et al., 2003; Goldfarb et al., 2005; Hart, 2007; Mathieu, 2021).

The CO_2-rich and low salinity nature of the hydrothermal fluids in the intrusion-related gold deposits has been proposed as the result of devolatilization of felsic magmas during their crystallization in a deeper environment (4 to 6 km), favoring its solubility and exsolution (Burrows et al., 1986; Thompson et al., 1999; Cline & Bodnar, 1991; Lowenstern, 2001; Sun et al., 2007).

According to Lang et al. (2000), the most prominent characteristics of this deposit type, besides their low saline CO_2-rich fluids, includes: 1. A genetic relationship with metaluminous, subalkalic intermediate to felsic intrusions with

an oxidation state spanning the boundary between the ilmenite and magnetite Ishihara (1977) series. 2. A metal assemblage including anomalous Bi, W, As, Mo, Te and/or Sb besides Au. 3. Restricted zones of hydrothermal alteration whiting the intrusions. 4. A continental setting inboard of the convergent plate boundaries and 5. Location in magmatic provinces with W-Sn mineral deposits. Interestingly, the most characteristic mineral style corresponds to a sub-parallel sheeted array of low sulfides quartz veins, although other styles also occur.

Conversely, orogenic gold deposits are typically developed along convergent margins during terrene accretion, translation or collision, in terranes which suffered moderate to high T and low to moderate P regional metamorphism (Powell et al., 1991; Groves et al., 2003; Goldfarb et al., 2005), in most of the cases spatially and temporally associated with granitic intrusions.

Orogenic gold deposits form typically in the latter part of the tectonic orogenesis being considered late-syntectonic, related to plate subduction and/or lithospheric delamination, involving the accretion of exotic terranes (Groves et al., 1998; Sillitoe & Thompson, 1998). This is the reason why they present a strong structural control involving faults or shear zones, normally of second or third order, as well as folds or areas presenting strong rheological contrasts (Groves et al., 2003; Goldfarb et al., 2005).

There is not a consensus about the origin of the hydrothermal fluids in the orogenic gold deposits nor the role of deep-magmatic processes, being the isotopic, fluid inclusions and dating evidences, not unequivocally distinct for a metamorphic or deep-magmatic source for this deposit type. Despite this and although a magmatic source is feasible, the associated intrusion bodies in most of the orogenic gold deposits are thought to be too small to provide the volume of fluid flow and to support the high gold tonnage in most of them (Groves et al., 2003). In this respect, available calculation of mineral equilibrium in the CaO-MgO-FeO-Al_2O_3-SiO_2 system showed that hydrous and carbonate minerals at 460-500°C in mid crustal levels, as the proposed source for a metamorphic origin for the hydrothermal fluids in orogenic deposits, are able to release voluminous low-salinity and CO_2-rich fluids (Powell et al., 1991).

In many cases, the differences between intrusion-related gold and orogenic gold deposits appear not to be only subtle but also difficult to be unequivocally tested. This is the case of the spatial, temporal and genetic relationship with intrusive bodies in the intrusion-related deposits or the late-syntectonic character for the orogenic gold model, with the additional complication of the commonly overprinting of the later in the former, as seems to occurs in the Abitibi Greenstone Belt, one of the world class golds producing metallogenic belts (Mathieu, 2021).

In Colombia, the biggest known intrusion-related gold deposit, Cerro Gramalote, locates in an E-W structural corridor, the so-called "Nus River Trend", crosscutting the roof of the post-collisional, 62 to 58 Ma age, Providencia tonalite facies of the Antioquia Batholith. There are discrete lodes and subparallel sheeted quartz-pyrite-sphalerite-galena-molybdenite veinlets containing significant amounts of Bi-sulfides and sulphosalts, as well as tellurides. These structures present narrow potassic K-Spar and sericite alteration haloes (Leal-Mejía, 2011; Leal-Mejía et al., 2019).

In Cerro Gramalote, age dating for the hydrothermal alteration and direct ore dating, as well as sulfur and lead isotopes clearly indicates a genetic relationship between mineralization and the hosting intrusive facies (Leal-Mejía, 2011).

In contrast, we showed here, that lodes and stockwork veinlet mineralization in the Ginebra Gold District, were formed slightly early in time than Cerro Gramalote and many other Antioquia-Sonsón batholiths gold occurences, during the late Cretaceous, about 67 to 65 Ma (**Figure 14**), nearly 25 Ma younger than the main facies of the Buga Batholith (Villagómez et al., 2011; Leal-Mejía, 2011; Leal-Mejía et al., 2019; Nivia et al., 2019) and temporally coeval with the Irra Stock (Leal-Mejía, 2011). This time period is coeval with a high-pressure and low-temperature orogenic metamorphism, recognized in the Jambaló blueschists, part of the Arquía Complex, in the western flank of the Central Cordillera (Bustamante & Bustamante, 2019), interpreted as the result of a dextral oblique convergence of the Caribbean Plate during the late Cretaceous-Paleocene.

In this context, it is possible to argue the Ginebra Gold District mineralizations emplaced in a strongly ductile to brittle structural environment, related to a dextral transpressive subduction to obduction tectonic episode, during a late syn-tectonic event related to the accretion of the Romeral terrane and probably in the sea-land of a subduction zone (Cediel et al., 2003; Villagómez et al., 2011; Leal-Mejía, 2011; Bustamante & Bustamante, 2019; Nivia et al., 2019). During this time there was emplaced the later facies of the Buga Batholith, coeval with small dacite to andesite porphyritic texture dikes (Brito et al., 2010; González, 2010; Nivia et al., 2019) (**Figure 14**).

As stated before, from the microthermometric and Raman analysis, the hydrothermal fluids responsible for gold mineralization in the Ginebra Gold District were low salinity, CO_2-rich and reduced, being the lodes and veins related to constrained sericite-chlorite haloes. Sulfur isotopes revealed a composition close to zero, suggesting a restricted fluid circulation through the magmatic rocks of the Buga Batholith and the Ginebra Ophiolitic Massif, probably controlled by the major fault systems in the area, in particular the Guabas-Pradera. It is also possible to argue from the oxygen and deuterium isotopes, a metamorphic origin for the hydrothermal fluids, which is in agreement with a metamorphic devolatilization process rather than a deep-magmatic source.

For all the mentioned characteristics, especially the nature of the hydrothermal fluids and the tectonic regime at the time of mineralization event, different as for example Cerro Gramalote, we propose the Ginebra Gold Disctrict mineralizations are more compatible with the orogenic gold type rather than to the intrusion-related origin.

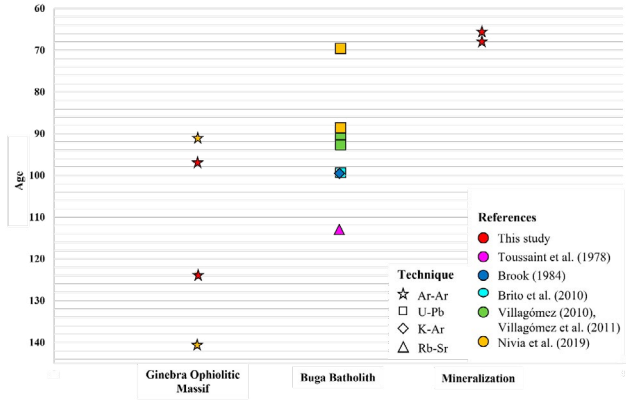

Figure 14. Age relationships for the Ginebra Gold District. The 123.57 Ma and 96.84 Ma ^{40}Ar-^{39}Ar hornblende dates for the Ginebra Ophiolitic Massif are coherent with a high-pressure oblique subduction-related metamorphism event, related to the Farallon Plate in the first case, while the second may be related to the syn-tectonic emplacement of the main Buga Batholith facies. The Late Cretaceous-Paleocene hydrothermal alteration dates for the Ginebra Gold District are coeval with the high-pressure metamorphism event produced by the Caribbean Plate convergence and subduction beneath the South American Plate.

Conclusions

Gold mineralization in the Ginebra District occurs as veins, disseminations and veinlet stockwork zones both in the Ginebra Ophiolitic Massif and the Buga Batholith, in strongly ductile to brittle deformed areas, in an approximate 6 km N-S trend. They characterize by a simple sulfide mineralogy assemblage in which fine grain size gold grains are related to scarce sulfides in at least two mineralizing events. Fluid inclusion and stable isotopic studies showed that the ore fluids were metamorphic in origin, low salinity, moderate to low temperature and CO_2-rich and an isothermal fluid mixing process as well as a H_2S loss process are proposed as the responsible for gold deposition.

^{40}Ar-^{39}Ar dating for the hydrothermal alteration haloes, coetaneous with gold deposition, indicates the mineralization occurred during the late Cretaceous to Paleocene, in a period characterized by a strong dextral transpressive subduction to obduction and exotic terrane accretion against the north-western part of the South American Plate. These characteristics are compatible with an Orogenic Gold deposit type.

Acknowledgments

This study is part of the project called 'Anteproyecto de investigación metalográfica, microtermométrica, geoquímica e isotópica para algunos

yacimientos minerales en Colombia', financed by Colciencias and the National University of Colombia. We would like to thank the Colombian Geological Survey SGC (INGEOMINAS), the United States Geological Survey (USGS) and the Technological Development Center of the Colombian Emerald (CDTEC) for allowing most of the analysis, in particular the Raman spectroscopy and the stable isotopes.

References

Aspden, J., & McCourt, W. (1986). Mesozoic oceanic terrane in the central Andes of Colombia. Geology, 14, 415-418. https://doi.org/10.1130/0091-7613(1986)14<415:MOTITC>2.0.CO;2

Bakker, R. J. (1997). Clathrates: Computer programs to calculate fluid inclusion V-X properties using clathrate melting temperatures. *Computers & Geosciences,* 23(1), 1-18. https://doi.org/10.1016/S0098-3004(96)00073-8

Bakker, R. J., & Brown, P. E. (2003). Computer modelling in fluid inclusion research. In: I. M. Samson, A. J. Anderson, & D. D. Marshall (Eds.). *Fluid Inclusions, Analysis and Interpretation.* Mineralogical Association of Canada, 32, pp. 175-212.

Barrera-Cortes, M. & Molano, J. C. (2021). Characterization of hydrothermal events associated with the occurrence of copper molybdenum minerals in the El Chucho creek at Cerrito, Valle del Cauca-Colombia. *Earth Sciences Research Journal*, 25(1), 5-12. https://doi.org/10.15446/esrj.v25n1.79152

Brito, R., Molano, J., Rodrigues, J., Dorado, C., Rodríguez, B. P., & Duarte, P. (2010). *U-Pb LA-ICPMS dating of the Buga Batholith and associated Porphyry dykes of the Ginebra Ofiolite–Westernmost Central Cordillera-Colombia*. VII South American Symposium on Isotope Geology vol. 2, Brasilia, Brazil, pp. 252-256.

Brook, M. (1984). *New Radiometric Age Data from S.W. Colombia.* Informe 1959-4. Ingeominas, Cali.

Burke, E. A. (2001). Raman microspectrometry of fluid inclusions. *Lithos,* 55(1-4), 139-158. https://doi.org/10.1016/S0024-4937(00)00043-8

Burrows, D. R., Wood, P. C., & Spooner, E. T. (1986). Carbon isotope evidence for a magmatic origin for Archaean gold-quartz vein ore deposits. *Nature,* 321(6073), 851-854. https://doi.org/10.1038/321851a0

Bustamante, C., & Bustamante, A. (2019). Two Cretaceous subduction events in the Central Cordillera: Insights from the high P–low T metamorphism. In: Gómez, J., & Pinilla–Pachon, A. O. (Eds.). *The Geology of Colombia.* Volume 2 Mesozoic. Servicio Geológico Colombiano, Publicaciones Geológicas Especiales 36, p. 485–498. Bogotá. https://doi.org/10.32685/pub.esp.36.2019.14

Czamanske, K., & Rye, R. (1974). Experimentally determined sulfur isotope fractionations between sphalerite and galena in the temperature range 600° to 275°C. *Economic Geology,* 69, 17-25. https://doi.org/10.2113/gsecongeo.69.1.17

Cediel, F., Shaw, R., & Cáceres, C. (2003). Tectonic assembly of the Northern Andean Block. In: C. Bartolini, R. T. Buffler, and J. Blickwede (Eds.). *The Circum-Gulf of Mexico and the Caribbean: Hydrocarbon habitats, basin formation, and plate tectonics*. AAPG Memoir 79, 815–848.

Cervera, J., & Garcés, A. (2005). *Estudio Metalográfico de las mineralizaciones auríferas en los sectores Cueva Loca y El Retiro (Departamento del Valle del Cauca), orientado al mejoramiento del proceso de beneficio.* [Dissertation Universidad Nacional de Colombia, Departamento de Geociencias.] Bogotá.

Cline, J. S., & Bodnar, R. J. (1991). Can economic porphyry copper mineralization be generated by a typical calc-alkaline melt? *Journal of Geophysical Research: Solid Earth,* 96(B5), 8113-8126. https://doi.org/10.1029/91JB00053

Diamond, L. W. (1990). Fluid inclusion evidence for P-V-T-X evolution of hydrothermal solutions in Late-Alpine gold-quartz veins at Brusson, Val d'Ayas, NW Italian Alps. *American Journal of Science, 290*, 912-958. https://doi.org/10.2475/ajs.290.8.912

Duan, Z., Moller, N., & Weare, J. H. (1992). An equation of state for the CH_4-CO_2-H_2O system: II. Mixtures from 50 to 1000°C and 0 to 1000 bar. *Geochimica et Cosmochimica Acta*, 56(7), 2619–2631. http://dx.doi.org/10.1016/0016-7037(92)90348-M

Frezzotti, M. L., Tecce, F., & Casagli, A. (2012). Raman spectroscopy for fluid inclusion analysis. *Journal of Geochemical Exploration,* 112, 1-20. https://doi.org/10.1016/j.gexplo.2011.09.009

Gebre-Mariam, M., Groves, D., McNaughton, N., Mikucki, E. & Vearncombe, J. (1993). Archaean Au-Ag mineralisation at Racetrack, near Kalgoorlie, Western Australia: a high crustal-level expression of the Archaean composite lodegold system. *Mineralium Deposita,* 28, 375–387. https://doi.org/10.1007/BF02431597

Goldfarb, R., Baker, T., Dubé, B., Groves, D., Hart, C., & Gosselin, P. (2005). Distribution, character, and genesis of gold deposits in metamorphic terranes. In: Hedenquist, J. W., Thompson, J. F. H., Goldfarb, R. J., & Richards, J. P. (Eds.). *100th Anniversary Volume*. Society of Economic Geologists, 407-457. https://doi.org/10.5382/AV100.14

Goldstein, R. H. (2003). Petrographic analysis of fluid inclusions. In: I. Samson, A. Anderson & D. Marshal (Eds.) *Fluid inclusion analysis and interpretation*. Short Course Series 32, Vancouver-British Columbia, p. 9-54.

González, H. I. (2010). *Geoquímica, geocronología de las unidades litológicas asociadas al sistema de Fallas Cauca-Romeral, Sector Centro-Sur*. Tomo 1. Proyecto Cordillera Occidental, Ingeominas. Colombia.

Groves, D. (1993). The crustal continuum model for late-Archaean lode-gold deposits of the Yilgarn Block, Western Australia. *Mineralium Deposita,* 28, 366–374. https://doi.org/10.1007/BF02431596

Groves, D., Goldfarb, R., Gebre-Mariam, M., Hagemann, S., & Robert, F. (1998). Orogenic gold deposits: A proposed classification in the context of their crustal distribution and relationship to other gold deposit types. *Ore Geology Reviews,* 13(1-5), 7-27. https://doi.org/10.1016/S0169-1368(97)00012-7

Groves, D., Goldfarb, R., Robert, F., & Hart, C. (2003). Gold Deposits in Metamorphic Belts: Overview of Current Understanding, Outstanding Problems, Future Research, and Exploration Significance. *Economic Geology*, 98, 1-29. https://doi.org/10.2113/gsecongeo.98.1.1

Hart, C. J. R. (2007). Reduced intrusion-related gold systems. In: Goodfellow, W. D. (Ed.). *Mineral deposits of Canada: A Synthesis of Major Deposit Types, District Metallogeny, the Evolution of Geological Provinces, and Exploration Methods*. Geological Association of Canada, Mineral Deposits Division, Special Publication No. 5, p. 95-112.

Hayashi, K., & Ohmoto, H. (1991). Solubility of gold in NaCl-and H2S-bearing aqueous solutions at 250–350°C. *Geochimica et Cosmochimica Acta,* 55(8), 2111-2126. https://doi.org/10.1016/0016-7037(91)90091-I

Ishihara, S. (1977). The magnetite-series and ilmenite-series granitic rocks. *Mining Geology,* 27, 293-305.

Jia, Y., Li, X., & Kerrich, R. (2000). A fluid inclusion study of Au-bearing quartz vein systems in the Central and North Deborah deposits of the Bendigo gold field, Central Victoria, Australia. *Economic Geology*, 95, 467- 494. https://doi.org/10.2113/gsecongeo.95.3.467

Kajiwara, Y., & Krouse, H. R. (1971). Sulfur Isotope Partitioning in Metallic Sulfide Systems. *Canadian Journal of Earth Sciences*, 8(11), 1397–1408. https://doi.org/10.1139/e71-129

Kerr, A., Marriner, G., Tarney, J., Nivia, A., Saunders, A., Thirwall, F., & Sinton, C. (1997). Cretaceous basaltic terranes in Western Colombia: Elemental, chronological and Sr-Nd isotopic constraints on petrogenesis. *Journal of Petrology,* 38(6), 677-702. https://doi.org/10.1093/petroj/38.6.677

Kerr, A. C., Tarney, J., Kempton, P. D., Spadea, P., Nivia, A., Marriner, G. F. & Duncan, R. A. (2002). Pervasive mantle plume head heterogeneity: Evidence from the late Cretaceous Caribbean-Colombian oceanic plateau. *Journal of Geophysical Research: Solid Earth,* 107. https://doi.org/10.1029/2001JB000790

Lang, J. R., Baker, T., Hart, C. J. R., & Mortensen, J. K. (2000). An exploration model for intrusion-related gold systems. *Society of Economic Geologists Newsletter*, 40, 6-15. https://doi.org/10.5382/SEGnews.2000-40.fea

Leal-Mejía, H. (2011). *Phanerozoic Gold Metallogeny in the Colombian Andes: A Tectono-Magmatic.* [Ph. D. thesis. Universitat de Barcelona], Barcelona, Spain.

Leal-Mejía, H., Shaw, R. P., & I Draper, J. C. M. (2019). Spatial-Temporal Migration of Granitoid Magmatism and the Phanerozoic Tectono-Magmatic Evolution of the Colombian Andes. In: Cediel, F., & Shaw, R. (Eds.). *Geology and Tectonics of Northwestern South America.* Switzerland: Springer Nature, pp. 253-410. https://doi.org/10.1007/978-3-319-76132-9_5

López, J. A., Leal-Mejía, H., Luengas, C. S., Velásquez, L. E., Celada, C. M., Sepúlveda, M. J., Prieto, D. A., Gómez, M., Hart, C. J. R. (2018). *Mapa Metalogénico de Colombia*. Bogotá: Servicio Geológico Colombiano.

Lowenstern, J. B. (2001). Carbon dioxide in magmas and implications for hydrothermal systems. *Mineralium Deposita,* 36, 490–502. https://doi.org/10.1007/s001260100185

Manco, J. (2020). *Geology, geochronology and geochemistry of the El Alacrán deposit, San Matías district, Córdoba-Colombia.* [M.Sc. thesis: University of British Columbia.] Vancouver, Canada.

Mathieu, L. (2021). Intrusion-Associated Gold Systems and Multistage Metallogenic Processes in the Neoarchean Abitibi Greenstone Belt. *Minerals,* 11(3), 261. https://doi.org/10.3390/min11030261

McCourt, W. J. (1984). *The Geology of the Central Cordillera the Department of Valle Del Cauca, Quindio and (N.W.) Tolima (Sheets 243, 261, 262, 280, 300).* Ingeominas, Cali.

McCourt, W. J., Aspden, J. A. & Brook, M. (1984). New geological and geochronological data from the Colombian Andes: continental growth by multiple accretion. Journal of the Geological Society, 141, 831–845. https://doi.org/10.1144/gsjgs.141.5.0831

McCourt, W. J., Millar, D., & Espinosa, A. (1985). *Geología de la Plancha 280–Palmira. Escala 1:100.000*. Ingeominas. Bogotá.

Molano, J. C., Londoño, J. I., Mosquera, G., Bacca, H., Cañón, Y., Londoño, S., Mojica, J., Pérez, O., Castro, A., & López, P. (2000). *Caracterización Mineralúrgica del Distrito Aurífero de Ginebra*. Proyecto de Investigación en Procesamiento de Minerales. Ingeominas, Cali.

Nivia, A. (2001). *Memoria Explicativa del Mapa Geológico del Departamento del Valle del Cauca.* Ingeominas, Bogotá.

Nivia, A., Tarazona, C., Paz, D., Ríos, J., Melo, A., Patiño, H., Torres, E., & Montoya, A. (2019). *Geología de las planchas 261 y 280 en los sectores de afloramiento del Macizo Ofiolítico de Ginebra y el Batolito de Buga.* Servicio Geológico Colombiano, 530

Ossa, C. (2006). *Petrogénesis de las rocas del Macizo Ofiolítico de Ginebra entre las veredas la Honda (Ginebra) y el Diamante (Buga) en el departamento del Valle del Cauca.* [Dissertation Universidad Nacional de Colombia. Facultad de Ciencias. Departamento de Geociencias]. Bogotá.

Peng, D. Y., & Robinson, D. B. (1976). A New Two-Constant Equation of State. *Industrial & Engineering Chemistry Fundamentals,* 15(1), 59-64.

Phillips, G. N., & Groves, D. I. (1983). The nature of Archaean gold-bearing fluids as deduced from gold deposits of Western Australia. Journal of the Geological Society of Australia, 30, 25–39. https://doi.org/10.1080/00167618308729234

Powell, R., Will, T., & Phillips, G. (1991). Metamorphism in Archaean greenstone belts: Calculated fluid compositions and implications for gold mineralization. *Journal of Metamorphic Geology,* 9(2), 141-150. https://doi.org/10.1111/j.1525-1314.1991.tb00510.x

Ramboz, C., Pichavant, M., & Weisbrod, A. (1982). Fluid immiscibility in natural processes: Use and misuse of fluid inclusion data: II. Interpretation of fluid inclusion data in terms of immiscibility. *Chemical Geology,* 37(1-2), 29-48. https://doi.org/10.1016/0009-2541(82)90065-1

Restrepo, J. J., & Toussaint, J. F. (1988). Terranes and continental accretion in the Colombian Andes. *Episodes,* 11, 189-193. https://doi.org/10.18814/epiiugs/1988/v11i3/006

Ridley, J., Mikucki, E., & Groves, D. (1996). Archean lode-gold deposits: Fluid flow and chemical evolution in vertically extensive hydrothermal systems. Ore Geology Reviews, 10(3-6), 279-293. https://doi.org/10.1016/0169-1368(95)00027-5

Robb, L. J. (2005). *Introduction to ore-forming processes*. Blackwell Science Ltd., 373 pp.

Rodríguez-Ramos, B. (2012). *Estudio metalogenético de las mineralizaciones auríferas del área de Ginebra y zonas aledañas, Valle del Cauca.* [Dissertation Universidad Nacional de Colombia. Facultad de Ciencias. Departamento de Geociencias.] Bogotá.

Roedder, A., & Bodnar, R. J. (2003). Geologic Pressure Determinations from Fluid Inclusion Studies. *Annual Review of Earth & Planetary Science*, 8, 263-301. https://doi.org/10.1146/annurev.ea.08.050180.001403

Roedder, E. (1984). *Fluid inclusions*. Mineralogical Society of America, 12, 644 pp.

Sakai, H. (1968). Isotopic properties of sulfur compounds in hydrothermal processes. *Geochemical Journal,* 2(1), 29-49. https://doi.org/10.2343/geochemj.2.29

Seward, T. (1973). Thio complexes of gold and the transport of gold in hydrothermal ore solutions. *Geochimica et Cosmochimica Acta,* 37(3), 379-399. https://doi.org/10.1016/0016-7037(73)90207-X

Seward, T. M. (1984). The transport and deposition of gold in hydrothermal systems. In: R. P. Foster (Ed.) *Gold'82: The geology, geochemistry and genesis of gold deposits,* 165-181.

Shenberger, D., & Barnes, H. (1989). Solubility of gold in aqueous sulfide solutions from 150 to 350°C. *Geochimica et Cosmochimica Acta,* 53(2), 269-278. https://doi.org/10.1016/0016-7037(89)90379-7

Sheppard, M. F. (1986). Characterization and isotopic variations in natural waters. *Reviews in Mineralogy,* 16, 165-183.

Sillitoe, R. H., & Thompson, J. F. (1998). Intrusion–Related Vein Gold Deposits: Types, Tectono-Magmatic Settings and Difficulties of Distinction from Orogenic Gold Deposits. *Resource Geology,* 48(4), 237-250. https://doi.org/10.1111/j.1751-3928.1998.tb00021.x

Stefánsson, A., & Seward, T. (2004). Gold(I) complexing in aqueous sulphide solutions to 500°C at 500 bar. *Geochimica et Cosmochimica Acta,* 68(20), 4121-4143. https://doi.org/10.1016/j.gca.2004.04.006

Sterner, S., & Bodnar, R. J. (1984). Synthetic fluid inclusions in natural quartz I. Compositional types synthesized and applications to experimental geochemistry. *Geochimica et Cosmochimica Acta,* 48(12), 2659-2668. https://doi.org/10.1016/0016-7037(84)90314-4

Sun, W., Binns, R., Fan, A., Kamenetsky, V., Wysoczanski, R., Wei, G., Hu, Y., & Arculus, R. (2007). Chlorine in submarine volcanic glasses from the eastern manus basin. *Geochimica et Cosmochimica Acta,* 71(6), 1542-1552. https://doi.org/10.1016/j.gca.2006.12.003

Suzuoki, T., & Epstein, S. (1976). Hydrogen isotope fractionation between OH-bearing minerals and water. *Geochimica et Cosmochimica Acta,* 40(10), 1229-1240. https://doi.org/10.1016/0016-7037(76)90158-7

Thompson, J., Sillitoe, R., Baker, T., Lang, J., & Mortensen, J. (1999). Intrusion-related gold deposits associated with tungsten-tin provinces. Mineralium Deposita, 34, 323–334. https://doi.org/10.1007/s001260050207

Toussaint, J., Botero, G., & Restrepo, J. (1978). *Datación K/Ar del Batolito de Buga, Colombia.* Universidad Nacional, Publicación Especial - Geología, 13, 1-3.

Toussaint, J. F. & Restrepo, J. J. (2020). Tectonostratigraphic terranes in Colombia: An update. Second part: Oceanic terranes. In: Gómez, J. & Pinilla–Pachon, A. O. (Eds.). *The Geology of Colombia, Volume 2 Mesozoic.* Servicio Geológico Colombiano. Publicaciones Geológicas Especiales 36, p. 237–260. Bogotá. https://doi.org/10.32685/pub.esp.36.2019.07

Villagómez, D., Spikings, R., Magna, T., Kammer, A., Winkler, W., & Beltrán, A. (2011). Geochronology, geochemistry and tectonic evolution of the Western and Central cordilleras of Colombia. *Lithos,* 125(3-4), 875-896. https://doi.org/10.1016/j.lithos.2011.05.003

Villagómez, D. (2010). *Thermochronology, geochronology and geochemistry of the Western and Central cordilleras and Sierra Nevada de Santa Marta, Colombia: the tectonic evolution of NW South America*. Département de Minéralogie, Université de Genève, Ph.D thesis.

Wilkinson, J. (2001). Fluid inclusions in hydrothermal ore deposits. *Lithos,* 55(1-4), 229-272. https://doi.org/10.1016/S0024-4937(00)00047-5

Zheng, Y. (1993). Calculation of oxygen isotope fractionation in hydroxyl-bearing silicates. *Earth and Planetary Science Letters,* 120(3-4), 247-263. https://doi.org/10.1016/0012-821X(93)90243-3